

Characteristic time of transition from write error to retention error in voltage-controlled magnetoresistive random-access memory [★]

Hiroko Arai*, Hiroshi Imamura

National Institute of Advanced Industrial Science and Technology (AIST), Research Center for Emerging Computing Technologies, Tsukuba, Ibaraki, 305-8568, Japan

arXiv:2303.05706v1 [cond-mat.mes-hall] 10 Mar 2023

Abstract

Voltage controlled magnetoresistive random access memory (VC MRAM) is a promising candidate for a future low-power high-density memory. The main causes of bit errors in VC MRAM are write error and retention error. As the size of the memory cell decreases, the data retention time decreases, which causes a transition from the write-error-dominant region to the retention-error-dominant region at a certain operating time. Here we introduce the characteristic time of the transition from the write-error-dominant region to the retention-error-dominant region and analyze how the characteristic time depends on the effective anisotropy constant, K_0 . The characteristic time is approximately expressed as $t_c = 2w\tau$, where w is the write error rate, and τ is the relaxation time derived by Kalmkov [J. Appl. Phys. 96, (2004) 1138-1145]. We show that for large K_0 , t_c increases with increase of K_0 similar to τ . The characteristic time is a key parameter for designing the VC MRAM for the variety of applications such as machine learning and artificial intelligence.

Keywords: voltage-control MRAM, write error, retention error

1. Introduction

Keeping information for enough time to ensure the reliability for computing is a key policy of the modern computing systems based on so-called the von Neumann architecture. Hierarchical memory system with cache, main memory, and storage has been successfully realized an effective and reliable computing [1, 2]. However, the performance of the von Neumann architecture is limited not only by the performance of the central processing unit (CPU) but by the data transfer rate between the memory and the CPU through the system bus, which is known as the von Neumann bottleneck.

In-memory computing is a promising approach to alleviate the von Neumann bottleneck, where resistive memory devices are used for both processing and memory [2, 3]. In-memory computing generally requires fast, high-density, low-power, scalable resistive memory devices, such as resistive random access memory (ReRAM) [4, 5], phase-change memory (PCM) [6–9], ferroelectric RAM (FeRAM) [10], and magnetoresistive RAM (MRAM) [11–18]. A crosspoint array of these resistive memory devices provides a hardware accelerator for the matrix-vector multiplication (MVM).

Recently much attention has been focused on the in-memory computing because it provides a powerful MVM tool for machine learning tasks such as image recognition, object detection, voice recognition, and time-series data analysis [7, 19, 20].

[★]This work was partly supported by JSPS KAKENHI Grant Number JP19H01108, and JP20K12003.

*corresponding author

Email addresses: arai-h@aist.go.jp (Hiroko Arai), h-imamura@aist.go.jp (Hiroshi Imamura)

Because the final outputs of these machine learning tasks are provided as a probability and its algorithms are error tolerant [21, 22], the accuracy required for the memory is not very high to obtain a practical result. T. Hirtzlin et al. showed that up to 0.1% bit error rate can be tolerated with little impact on recognition performance of a standard binary neural network [23].

Voltage-control (VC) MRAM is a promising candidate for the key element of the fast and low-power in-memory computing because of the fast (~ 0.1 ns) and low-power (~ 1 fJ) writing [24–32]. The VC MRAM uses the voltage control of magnetic anisotropy (VCMA) effect [24, 26, 33–35] to induce the precession of magnetization for writing, and little Joule heating is generated.

The main causes of bit errors in VC MRAM are write error and retention error. The write error in VC MRAM is a failure in magnetization switching due to thermal agitation field during the precession and relaxation. The write error rate (WER) of the VC MRAM is of the order of 10^{-6} [29] which is low enough to obtain practical recognition accuracy. The retention error in VC MRAM is an accidental switching of magnetization that occurs while retaining the data. The origin of the retention error is also thermal agitation field. The retention error rate (RER) of the VC MRAM can be calculated by solving the Fokker-Planck equation as shown in Ref. [37]. As the size of the memory cell decreases, the data retention time decreases, which causes a transition from the write-error-dominant region to the retention-error-dominant region at a certain operating time. For developing the fast and low-power in-memory computing it is important to know the characteristic time of the transition.

In this paper we define the characteristic time, t_c , of the tran-

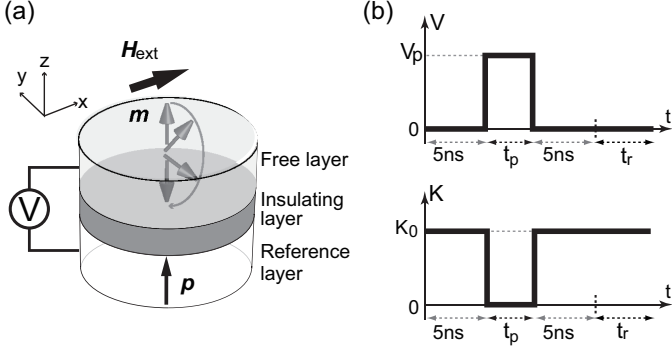


Figure 1: (a) Magnetic tunnel junction nanopillar and the definition of Cartesian coordinates (x, y, z) . The non-magnetic insulating layer is sandwiched by the two ferromagnetic layers: the free layer and the reference layer. A static magnetic field, \mathbf{H}_{ext} , is applied along the positive x direction. Application of the voltage, V , pulse can induce precessional motion of the magnetization in the free layer through the VCMA effect. (b) Time evolution of the voltage pulse V and the anisotropy constant K . Without application of voltage the effective anisotropy constant is K_0 . After 5 ns relaxation the voltage pulse with the magnitude of V_p is applied for the duration of t_p to reduce K to zero. After the pulse the magnetization is relaxed. The WER is calculated using the direction of magnetization at 5 ns after the pulse. The contribution from the retention error is estimated by analyzing the error rate after the relaxation for the extra relaxation time, t_r .

sition from the write-error-dominant region to the retention-error-dominant region and analyze the dependence of the characteristic time on the effective anisotropy constant, K_0 . We obtained the approximate expression of the characteristic and show that t_c increases with increase of K_0 for large value of K_0 .

2. Model and Methods

Figure 1(a) schematically shows the magnetic tunnel junction nanopillar which is the basic element of the VC MRAM. The nonmagnetic insulating layer is sandwiched by the two ferromagnetic layers called the free layer and the reference layer. The size of the MTJ nanopillar is assumed to be so small that the magnetization dynamics can be described by the macrospin model. We denote the direction of the magnetization in the free layer by the unit vector $\mathbf{m} = (m_x, m_y, m_z)$. Application of the voltage, V , pulse reduces the magnetic anisotropy through the VCMA effect and induces the precession of magnetization around the static external field, \mathbf{H}_{ext} , applied in the positive x direction. The magnetization unit vector in the reference layer, \mathbf{p} , is fixed to the positive z direction, i.e. $\mathbf{p} = (0, 0, 1)$. The information stored in the VC MRAM is read as the change of the tunnel resistance due to the tunnel magnetoresistance effect [38–41].

Figure 1(b) shows the shape of the voltage pulse and the corresponding time evolution of the effective anisotropy constant, K , in our simulations. The initial direction of \mathbf{m} at $t = 0$ is set to the equilibrium direction with $m_z > 0$, which minimizes the energy density

$$E = K_0(1 - m_z^2) - \mu_0 M_s H_{\text{ext}} m_x, \quad (1)$$

where K_0 is the effective anisotropy constant of the free layer at $V = 0$, which consists of the crystal magnetic anisotropy

and the demagnetizing energy density, μ_0 is the permeability of vacuum, M_s is the saturation magnetization. For the first 5 ns, the initial state are thermalized by the thermal agitation field to obey the Boltzmann distribution at temperature, T . During the thermalization no voltage is applied, and the effective anisotropy constant is K_0 . Then the voltage pulse with the magnitude of V_p is applied for the duration of t_p . During the pulse the effective anisotropy constant is zero, and the magnetization precesses around the external magnetic field. The pulse width, t_p , is set to a half of the precession period to switch the magnetization. After the pulse the magnetization is relaxed under the condition of $K = K_0$. The WER is calculated using the direction of magnetization at 5 ns after the end of the pulse. The contribution from the retention error is estimated by analyzing the error rate after the relaxation for the extra relaxation time, t_r .

Temporal evolution of \mathbf{m} is obtained by solving the Landau-Lifshitz-Gilbert (LLG) equation,

$$\frac{d\mathbf{m}}{dt} = -\gamma \mathbf{m} \times \mathbf{H}_{\text{eff}} + \alpha \mathbf{m} \times \frac{d\mathbf{m}}{dt}, \quad (2)$$

where γ is the gyromagnetic constant and α is the Gilbert damping constant. The first and second terms on the right hand side represent the torque resulting from the effective field, \mathbf{H}_{eff} , and the damping torque, α respectively. The effective field comprises the external field, anisotropy field, \mathbf{H}_{anis} , and thermal agitation field, $\mathbf{H}_{\text{therm}}$, as

$$\mathbf{H}_{\text{eff}} = \mathbf{H}_{\text{ext}} + \mathbf{H}_{\text{anis}} + \mathbf{H}_{\text{therm}}. \quad (3)$$

The anisotropy field is defined as

$$\mathbf{H}_{\text{anis}} = \frac{2K(t)}{\mu_0 M_s} m_z(t) \mathbf{e}_z, \quad (4)$$

where \mathbf{e}_z is the unit vector in the positive z direction. The thermal agitation field is determined by the fluctuation-dissipation theorem [42–46] and satisfies the following relations

$$\langle \mathbf{H}_{\text{therm}}^i(t) \rangle = 0, \quad (5)$$

$$\langle \mathbf{H}_{\text{therm}}^i(t) \mathbf{H}_{\text{therm}}^j(t') \rangle = \xi \delta_{i,j} \delta(t - t'), \quad (6)$$

where $\langle \rangle$ denotes the statistical average, the indices i, j denote the x, y , and z components of the thermal agitation field. $\delta_{i,j}$ represents Kronecker's delta, and $\delta(t - t')$ represents Dirac's delta function. The coefficient ξ is given by

$$\xi = \frac{2\alpha k_B T}{\gamma \mu_0 M_s \Omega}, \quad (7)$$

where k_B is the Boltzmann constant, T is temperature, and Ω is the volume of the free layer. The WER is obtained by counting the number of failure in 10^7 trials of writing. The success or failure of each trial is determined by the sign of m_z at $t = t_p + 10$ ns [see Fig. 1(b)]. We also calculate the error rate after $t = t_p + 10$ ns by performing the same simulation until $t = t_p + t_r + 10$ ns.

The RER is the probability of the accidental switching of magnetization by thermal agitation during the period of data retention. We employ the theory of RER given by Kalmykov in Ref. [37], to save the simulation time, and to provide a theoretical analysis. Introducing the escape ratio, Γ , over the potential barrier which separate the two different equilibrium directions of the magnetization, the RER is given by the switching probability defined as

$$P(t) = \frac{1}{2} \left(1 - e^{-2\Gamma t}\right), \quad (8)$$

which is the solution of the master equation as

$$\frac{d}{dt}P(t) = -\Gamma P(t) + \Gamma(1 - P(t)). \quad (9)$$

The inverse of 2Γ is called the relaxation time and is denoted by τ , i.e., $\tau = 1/(2\Gamma)$.

Kalmykov derived the expressions of τ for three different dissipation regions: the very low damping (VLD, $\alpha < 0.001$) region, the intermediate-to-high damping (IHD, $\alpha \gg 1$) region, and the crossover ($0.01 < \alpha < 1$) region. For VC MRAM, the typical value of α is in the crossover region. The expression of τ in the crossover region is given by Eq. (18) in Ref. [37] as

$$\tau = \tau_{\text{IHD}} \frac{A(\alpha S_1 + \alpha S_2)}{A(\alpha S_1)A(\alpha S_2)}, \quad (10)$$

where

$$A(\alpha S_i) = \exp \left[\frac{1}{\pi} \int_0^\infty \frac{\ln[1 - \exp\{-\alpha S_i(x^2 + 1/4)\}]}{x^2 + 1/4} dx \right], \quad (11)$$

$$\tau_{\text{IHD}} \sim \frac{2\tau_N \pi \sqrt{h} e^{\sigma(1-h)^2}}{\sigma \sqrt{1+h}(1-2h + \sqrt{1+4h(1-h)/\alpha^2})}, \quad (12)$$

and

$$S_i = 16\sigma \sqrt{h} \left[1 - \frac{13}{6}h + \frac{11}{8}h^2 - \frac{3}{16}h^3 + \frac{7}{384}h^4 + \frac{h^5}{256} + O(h^6) \right]. \quad (13)$$

Here, $\tau_N = \beta M_s(1 + \alpha^2)/(2\gamma\alpha)$, $h = \beta\mu_0 M_s H_{\text{ext}}/(2\sigma)$, $\sigma = \beta K$, and $\beta = \Omega/(k_B T)$. The index of S_i is the label of the equilibrium directions, e.g., "1" for $m_z > 0$ and "2" for $m_z < 0$. Since the system we consider has an inversion symmetry with respect to the $x - y$ plane, i.e., $z \rightarrow -z$, Eq. (10) can be expressed as $\tau = \tau_{\text{IHD}} A(2\alpha S_1)/A(\alpha S_1)^2$.

The following parameters are assumed. The saturation magnetization is $M_s = 0.955$ MA/m [36], and the pulse width is $t_p = 0.18$ ns. The magnitude of the external field is $H_{\text{ext}} = 1$ kOe. The diameter and thickness of the free layer are 40 nm and 1.1 nm, respectively. The Gilbert damping constant $\alpha = 0.1$, and temperature is $T = 300$ K.

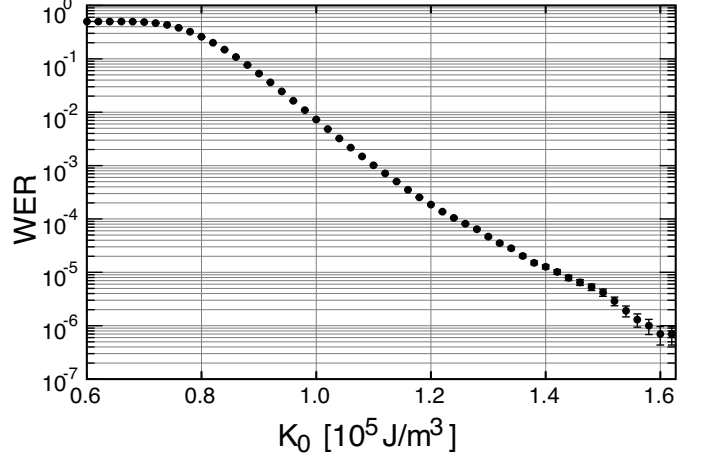


Figure 2: WER as a function of anisotropy constant, K_0 . The dot represents the mean of the WER, and the error bar stands for the standard deviation of the WER. Each data points are obtained by averaging the results of 10^7 trials.

3. Results

Figure 2 shows K_0 dependence of the WER, where the dot represents the mean of the WER, and the error bar stands for the standard deviation of the WER. Each data points are obtained by averaging the results of 10^7 trials. The WER is about 0.5 for small K_0 (< 0.8) because the anisotropy energy is too small to retain the direction of the initial magnetization for 5 ns. The magnetization is almost equally distributed around the equilibrium directions with $m_z > 0$ and $m_z < 0$ at the beginning of the pulse. In other words, the retention time is less than 5 ns. For $K_0 > 0.8$, the WER exponentially decreases with increase of K_0 and reaches below 10^{-6} at $K_0 = 1.6 \times 10^5$ J/m³.

Figure 3 shows an example of the typical t_r -dependence of the error rate. The effective anisotropy constant is assumed to be $K_0 = 1.0 \times 10^5$ J/m³. The dots connected by the solid curve represents the results obtained by numerically solving the LLG equation. The gray horizontal solid line indicates the value of the WER: 7.3×10^{-3} . The Dashed curve represents the RER of Eq. (8). For short t_r , the error rate is much larger than the RER and is dominated by the WER. For large t_r , the error rate converges to the RER, i.e., the RER dominates the error rate. We introduce the characteristic time, t_c , for transition from the write-error-dominant region to the retention-error-dominant region as the intersection point of the dashed curve and the gray horizontal solid line, as shown in Fig. 3.

Since the RER equals to WER at $t_r = t_c$, we have

$$t_c = \tau \ln \frac{1}{1 - 2w}, \quad (14)$$

where w denotes the WER. Assuming that $w \ll 1$, Eq. (14) is approximated as

$$t_c \approx 2w\tau. \quad (15)$$

The K_0 -dependence of t_c is determined by the K_0 -dependence of w and τ . The K_0 -dependence of w is already shown in Fig. 2. w decreases exponentially with increase of K_0 .

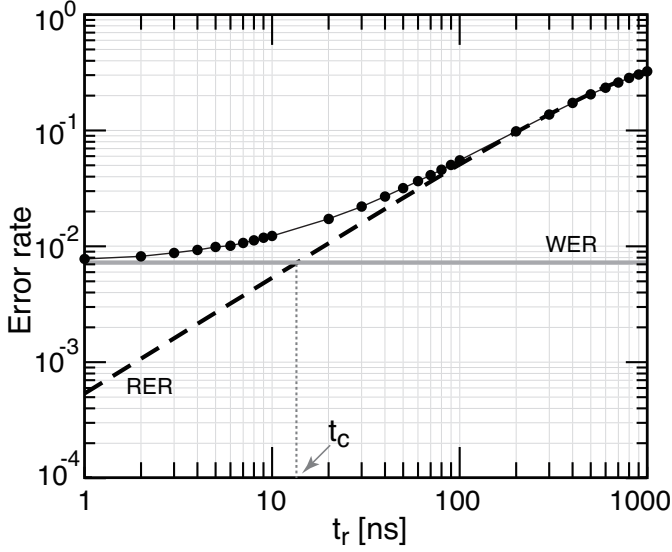


Figure 3: Dependence of the error rate on t_r for $K = 1.0 \times 10^5$. The dots represent the results obtained by numerically solving the LLG equation. The thin solid curve connecting the dots is the guide for eyes. The dashed curve represents the RER of Eq. (8). The gray horizontal solid line indicates the value of WER: 7.3×10^{-3} . The intersection point between the gray horizontal line and the dashed line defines the characteristic time for transition from the write-error-dominant region to the retention-error-dominant region, t_c . The write-error-dominant region is $t_r < t_c$, and the retention-error-dominant region is $t_r > t_c$.

The K_0 -dependence of τ is shown in Fig. 4(a). On contrary to the K_0 -dependence of w , τ increases with increase of K_0 . The K_0 -dependence t_c is determined by competition between the decreasing contribution from w and the increasing contribution from τ . Figure 4(b) shows the K_0 -dependence of t_c . The WER at each point shown in Fig. 2 is indicated by color. Although t_c is almost independent of K_0 for small K_0 (< 1.0), it exponentially increases with increase of K_0 for large K_0 (> 1.0) due to the exponential dependence of τ on K_0 shown in Fig. 4(a).

We focused on the influence of K_0 , which is the most important parameter of VC MRAM because of its operating principle. We briefly comment on the influence over t_c from another key parameter, the damping constant, α . With increase of α , the WER becomes larger. The present values for the pulse width and the pulse amplitude are the optimal values that minimize the WER. The increase of the WER results in the increase of t_c (see Fig. 3).

We also briefly comment on the RER of the other MRAM. The spin-transfer torque (STT) MRAM and spin-orbit torque (SOT) MRAM are principally does not required the application of an external magnetic field, unlike the VC MRAM. The analytical formula of the RER for STT/SOT-MRAM has been derived by Brown [42].

4. Summary

In summary, we study the characteristic time, t_c , of the transition from write-error-dominant region to retention-error-

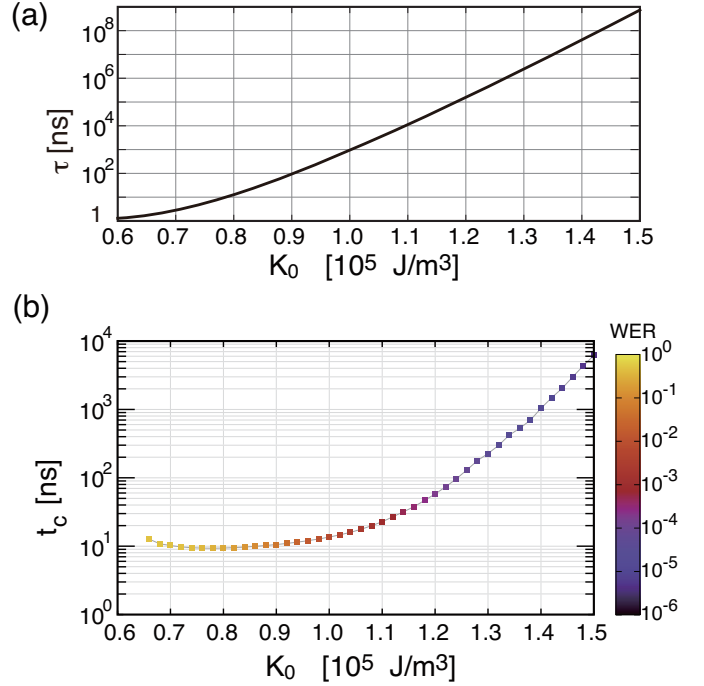


Figure 4: (a) K_0 -dependence of τ defined by Eq. (10). (b) K_0 -dependence of characteristic time t_c . Colors indicate the value of WER shown in Fig. 2.

dominant region in VC MRAM by paying special attention to the dependence of t_c on the effective anisotropy constant, K_0 . We show that the characteristic time is approximately expressed as $t_c = 2w\tau$, where w is the write error rate, and τ is the relaxation time derived by Kalmkov [37]. The K_0 -dependence of t_c is determined by competition between the K_0 -dependence of w and τ . We show that for large K_0 , t_c increases with increase of K_0 similar to τ . The characteristic time is a key parameter for designing the VC MRAM for the variety of applications such as machine learning and artificial intelligence because the working frequency should be higher than $1/t_c$ to ensure the practical recognition accuracy required.

Appendix A. Anisotropy constant dependence of half precession period of magnetization

In VC MRAM, the half precession period is an important parameter. We briefly discuss the dependence between the half precession period and the anisotropy constant.

For the analysis of the magnetization dynamics during the pulse, it is convenient to introduce the precession cone angle ξ and the precession angle η defined as $(m_x, m_y, m_z) = (\cos \xi \sin \eta, \sin \xi \cos \eta, \cos \xi \cos \eta)$, and the dimensionless time $\tau = \gamma H_{\text{ext}} t / (1 + \alpha^2)$. In terms of ξ and η , the LLG equation is expressed as

$$\dot{\xi} = -\alpha \sin \xi + \kappa \sin \xi \sin \eta (\cos \eta + \alpha \cos \xi \sin \eta), \quad (\text{A.1})$$

$$\dot{\eta} = 1 + \kappa \sin \eta (\alpha \cos \eta - \cos \xi \sin \eta), \quad (\text{A.2})$$

where $\kappa = 2K/(\mu_0 M_s H_{\text{ext}})$. The initial conditions are $\xi(0) = \arccos(1/\kappa_0)$ and $\eta(0) = \pi/2$, where $\kappa_0 = 2K_0/(\mu_0 M_s H_{\text{ext}})$. In

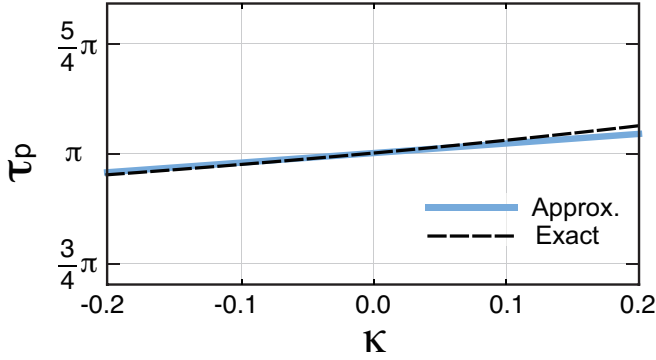


Figure A.1: The values of (τ_p, κ) satisfying $\eta = 3\pi/2$. The blue solid curve shows the approximate result given by Eq. (A.4). The black dashed curve represents the exact result obtained by numerically solving Eqs. (A.1) and (A.2) with $\eta(\tau_p) = 3\pi/2$.

the case of $K = 0$, i.e., $\kappa = 0$, the analytical solutions of ξ and η are available, which represent the damped precession with a spiral trajectory. The precession angle at the end of pulse, $\tau = \tau_p$, corresponding to $t = t_p$, is given by $\eta = \pi/2 + \tau_p$. The half precession period is $\tau_p = \pi$ ($t_p = 180$ ps in SI unit).

The K dependence of precession period during the pulse in the vicinity of $K = 0$ is analyzed by using the perturbation theory. Expanding the solutions of Eqs. (A.1) and (A.2) up to the first order of κ and neglecting the term with $\alpha\kappa$, we obtain

$$\eta(\tau) \sim \frac{\pi}{2} + \tau - \frac{\kappa}{4\kappa_0} \{2\tau + \sin(2\tau)\}. \quad (\text{A.3})$$

The pulse duration for half of precession period is obtained by solving $\eta(\tau) = 3\pi/2$ with the linear approximation of $\sin(2\tau)$ around $\tau = \pi$ as

$$\tau_p^H = \pi \left(1 + \frac{\kappa}{2\kappa_0} \right). \quad (\text{A.4})$$

τ_p^H is an increasing function of κ .

Figure A.1 shows the value of (τ_p, κ) satisfying $\eta = 3\pi/2$. The blue thick solid curve shows the approximate result of Eq. (A.4). The black dashed curve shows the exact result obtained by numerically solving Eqs. (A.1) and (A.2) with $\eta(\tau_p) = 3\pi/2$. The approximate result of Eq. (A.4) agrees well with the exact numerical result.

References

- [1] S. Wang, X. Liu, P. Zhou, **The Road for 2D Semiconductors in the Silicon Age**, *Advanced Materials* 34 (2022) 2106886. <https://doi.org/10.1002/adma.202106886>
- [2] A. Sebastian, M. Le Gallo, R. Khaddam-Aljameh, E. Eleftheriou, **Memory devices and applications for in-memory computing**, *Nat. Nanotech.* 15 (2020) 529–544. <https://doi.org/10.1038/s41565-020-0655-z>
- [3] D. Ielmini, H.-S. P. Wong, **In-memory computing with resistive switching devices**, *Nature Electronics* 1 (2018) 333–343. <https://doi.org/10.1038/s41928-018-0092-2>
- [4] R. Waser, M. Aono, **Nanoionics-based resistive switching memories**, *Nat. Mater.* 6 (2007) 833–840. <https://doi.org/10.1038/nmat2023>

- [5] Y. Chen, **ReRAM: History, Status, and Future**, *IEEE Transactions on Electron Devices* 67 (2020) 1420–1433. <https://doi.org/10.1109/TED.2019.2961505>.
- [6] S. Raoux, W. Welnic, D. Ielmini, **Phase Change Materials and Their Application to Nonvolatile Memories**, *Chem. Rev.* 110 (2010) 240–267. <https://doi.org/10.1021/cr900040x>
- [7] G. W. Burr, R. M. Shelby, A. Sebastian, S. Kim, S. Kim, S. Sidler, K. Virwani, M. Ishii, P. Narayanan, A. Fumarola, L. L. Sanches, I. Boybat, M. Le Gallo, K. Moon, J. Woo, H. Hwang, Y. Leblebici, **Neuromorphic computing using non-volatile memory**, *Advances in Physics: X* 2 (2017) 89–124. <https://doi.org/10.1080/23746149.2016.1259585>
- [8] S. Slesazek, T. Mikolajick, **Nanoscale resistive switching memory devices: a review**, *Nanotechnology* 30 (2019) 352003. <https://doi.org/10.1088/1361-6528/ab2084>
- [9] V. Joshi, M. Le Gallo, S. Haefeli, I. Boybat, S. R. Nandakumar, C. Piveteau, M. Dazzi, B. Rajendran, A. Sebastian, E. Eleftheriou, **Accurate deep neural network inference using computational phase-change memory**, *Nat. Commun.* 11 (2020) 2473. <https://doi.org/10.1038/s41467-020-16108-9>
- [10] T. Mikolajick, C. Dehm, W. Hartner, I. Kasko, M. Kastner, N. Nagel, M. Moert, C. Mazure, **FeRAM technology for high density applications**, *Microelectronics Reliability* 41 (2001) 947–950. [https://doi.org/10.1016/S0026-2714\(01\)00049-X](https://doi.org/10.1016/S0026-2714(01)00049-X)
- [11] S. Yuasa, A. Fukushima, K. Yakushiji, T. Nozaki, M. Konoto, H. Maehara, H. Kubota, T. Taniguchi, H. Arai, H. Imamura, K. Ando, Y. Shiota, F. Bonell, Y. Suzuki, N. Shimomura, E. Kitagawa, J. Ito, S. Fujita, K. Abe, K. Nomura, H. Noguchi, H. Yoda, **Future prospects of MRAM technologies**, 2013 IEEE International Electron Devices Meeting (2013) 3.1.1–3.1.4. <https://doi.org/10.1109/IEDM.2013.6724549>
- [12] K. Ando, S. Fujita, J. Ito, S. Yuasa, Y. Suzuki, Y. Nakatani, T. Miyazaki, H. Yoda, **Spin-transfer torque magnetoresistive random-access memory technologies for normally off computing (invited)**, *J. Appl. Phys.* 115 (2014) 172607. <https://doi.org/10.1063/1.4869828>
- [13] A. D. Kent, D. C. Worledge, **A new spin on magnetic memories**, *Nat. Nanotech.* 10 (2015) 187–191. <https://doi.org/10.1038/nnano.2015.24>
- [14] D. Apalkov, B. Dieny, J. M. Slaughter, **Magnetoresistive Random Access Memory**, *Proceedings of the IEEE* 104 (2016) 1796–1830. <https://doi.org/10.1109/JPROC.2016.2590142>.
- [15] S. Jain, A. Ranjan, K. Roy, A. Raghunathan, **Computing in Memory With Spin-Transfer Torque Magnetic RAM**, *IEEE Transactions on Very Large Scale Integration (VLSI) Systems* 26 (2018) 470–483. <https://doi.org/10.1109/TVLSI.2017.2776954>.
- [16] L. Chang, X. Ma, Z. Wang, Y. Zhang, Y. Xie, W. Zhao, **PXNOR-BNN: In/With Spin-Orbit Torque MRAM Preset-XNOR Operation-Based Binary Neural Networks**, *IEEE Transactions on Very Large Scale Integration (VLSI) Systems* 27 (2019) 2668–2679. <https://doi.org/10.1109/TVLSI.2019.2926984>.
- [17] T. Nozaki, T. Yamamoto, S. Miwa, M. Tsujikawa, M. Shirai, S. Yuasa, Y. Suzuki, **Recent Progress in the Voltage-Controlled Magnetic Anisotropy Effect and the Challenges Faced in Developing Voltage-Torque MRAM**, *Micromachines* 10 (2019) 327. <https://doi.org/10.3390/mi10050327>
- [18] T.-N. Pham, Q.-K. Trinh, I.-J. Chang, M. Alioto, **STT-MRAM Architecture with Parallel Accumulator for In-Memory Binary Neural Networks**, *IEEE International Symposium on Circuits and Systems (ISCAS)*, (2021) 1–5. <https://doi.org/10.1109/ISCAS51556.2021.9401695>.
- [19] Y. LeCun, Y. Bengio, G. Hinton, **Deep learning**, *Nature* 521 (2015) 436–444. <https://doi.org/10.1038/nature14539>
- [20] J. Schmidhuber, **Deep learning in neural networks: An overview**, *Neural Networks* 61 (2015) 85–117. <https://doi.org/10.1016/j.neunet.2014.09.003>
- [21] C. Torres-Huitzil, B. Girau, **Fault and Error Tolerance in Neural Networks: A Review**, *IEEE Access* 5 (2017) 17322–17341. <https://doi.org/10.1109/ACCESS.2017.2742698>
- [22] M. Qin, C. Sun, D. Vucinic, **Improving Robustness of Neural Networks**

- against Bit Flipping Errors during Inference, *JOIG* 6 (2018) 181–186.
<https://doi.org/10.18178/joig.6.2.181-186>
- [23] T. Hirtzlin, B. Penkovsky, J.-O. Klein, N. Locatelli, A. F. Vincent, M. Bocquet, J.-M. Portal, D. Querlioz, **Implementing Binarized Neural Networks with Magnetoresistive RAM without Error Correction**, 2019 IEEE/ACM International Symposium on Nanoscale Architectures (NANOARCH) (2019) 1–5.
<https://doi.org/10.1109/NANOARCH47378.2019.181300>
- [24] T. Maruyama, Y. Shiota, T. Nozaki, K. Ohta, N. Toda, M. Mizuguchi, A. A. Tulapurkar, T. Shinjo, M. Shiraishi, S. Mizukami, Y. Ando, Y. Suzuki, **Large voltage-induced magnetic anisotropy change in a few atomic layers of iron**, *Nat. Nanotech.* 4 (2009) 158–161.
<https://doi.org/10.1038/nnano.2008.406>
- [25] J. J. Nowak, R. P. Robertazzi, J. Z. Sun, G. Hu, D. W. Abraham, P. L. Trouilloud, S. Brown, M. C. Gaidis, E. J. O’Sullivan, W. J. Gallagher, D. C. Worledge, **Demonstration of ultralow bit error rates for spin-torque magnetic random-access memory with perpendicular magnetic anisotropy**, *IEEE Magn. Lett.* 2 (2011) 3000204.
<https://doi.org/10.1109/LMAG.2011.2155625>
- [26] Y. Shiota, T. Nozaki, F. Bonell, S. Murakami, T. Shinjo, Y. Suzuki, **Induction of coherent magnetization switching in a few atomic layers of FeCo using voltage pulses**, *Nat. Mater.* 11 (2012) 39–43.
<https://doi.org/10.1038/nmat3172>
- [27] C. Grezes, F. Ebrahimi, J. G. Alzate, X. Cai, J. A. Katine, J. Langer, B. Ocker, P. Khalili Amiri, K. L. Wang, **Ultra-low switching energy and scaling in electric-field-controlled nanoscale magnetic tunnel junctions with high resistance-area product**, *Appl. Phys. Lett.* 108 (2016) 012403.
<https://doi.org/10.1063/1.4939446>
- [28] S. Kanai, F. Matsukura, H. Ohno, **Electric-field-induced magnetization switching in CoFeB/MgO magnetic tunnel junctions with high junction resistance**, *Appl. Phys. Lett.* 108 (2016) 192406.
<https://doi.org/10.1063/1.4948763>
- [29] T. Yamamoto, T. Nozaki, H. Imamura, Y. Shiota, S. Tamaru, K. Yakushiji, H. Kubota, A. Fukushima, Y. Suzuki, S. Yuasa, **Improvement of write error rate in voltage-driven magnetization switching**, *J. Phys. D: Appl. Phys.* 52 (2019) 164001.
<https://doi.org/10.1088/1361-6463/ab03c2>
- [30] R. Matsumoto, H. Imamura, **Methods for reducing write error rate in voltage-induced switching having prolonged tolerance of voltage-pulse duration**, *AIP Advances* 9 (2019) 125123.
<https://doi.org/10.1063/1.5128154>
- [31] T. Yamamoto, T. Nozaki, H. Imamura, S. Tamaru, K. Yakushiji, H. Kubota, A. Fukushima, Y. Suzuki, S. Yuasa, **Voltage-Driven Magnetization Switching Using Inverse-Bias Schemes**, *Phys. Rev. Applied* 13 (2020) 014045.
<https://doi.org/10.1103/PhysRevApplied.13.014045>
- [32] R. Matsumoto, H. Imamura, **Low-Power Switching of Magnetization Using Enhanced Magnetic Anisotropy with Application of a Short Voltage Pulse**, *Phys. Rev. Applied* 14 (2020) 021003.
<https://doi.org/10.1103/PhysRevApplied.14.021003>
- [33] M. Weisheit, S. Fähler, A. Marty, Y. Souche, C. Poinsignon, D. Givord, **Electric Field-Induced Modification of Magnetism in Thin-Film Ferromagnets**, *Science* 315 (2007) 349–351.
<https://doi.org/10.1126/science.1136629>
- [34] T. Nozaki, Y. Shiota, M. Shiraishi, T. Shinjo, Y. Suzuki, **Voltage-induced perpendicular magnetic anisotropy change in magnetic tunnel junctions**, *Appl. Phys. Lett.* 96 (2010) 022506.
<https://doi.org/10.1063/1.3279157>
- [35] S. Miwa, M. Suzuki, M. Tsujikawa, K. Matsuda, T. Nozaki, K. Tanaka, T. Tsukahara, K. Nawaoka, M. Goto, Y. Kotani, T. Ohkubo, F. Bonell, E. Tamura, K. Hono, T. Nakamura, M. Shirai, S. Yuasa, Y. Suzuki, **Voltage controlled interfacial magnetism through platinum orbits**, *Nat. Commun.* 8 (2017) 15848.
<https://doi.org/10.1038/ncomms15848>
- [36] T. Yamamoto, T. Nozaki, H. Imamura, Y. Shiota, T. Ikeura, S. Tamaru, K. Yakushiji, H. Kubota, A. Fukushima, Y. Suzuki, S. Yuasa, **Write-Error Reduction of Voltage-Torque-Driven Magnetization Switching by a Controlled Voltage Pulse**, *Phys. Rev. Applied* 11 (2019) 014013.
<https://doi.org/10.1103/PhysRevApplied.11.014013>
- [37] Y. P. Kalmykov, **The relaxation time of the magnetization of uniaxial single-domain ferromagnetic particles in the presence of a uniform magnetic field**, *J. Appl. Phys.* 96 (2004) 1138–1145.
<https://doi.org/10.1063/1.1760839>
- [38] M. Julliere, **Tunneling between ferromagnetic films**, *Phys. Lett. A* 54 (1975) 225–226.
[https://doi.org/10.1016/0375-9601\(75\)90174-7](https://doi.org/10.1016/0375-9601(75)90174-7)
- [39] T. Miyazaki, N. Tezuka, **Giant magnetic tunneling effect in Fe/Al₂O₃/Fe junction**, *J. Magn. Magn. Mat.* 139 (1995) L231–L234.
[https://doi.org/10.1016/0304-8853\(95\)90001-2](https://doi.org/10.1016/0304-8853(95)90001-2)
- [40] S. Yuasa, T. Nagahama, A. Fukushima, Y. Suzuki, K. Ando, **Giant room-temperature magnetoresistance in single-crystal Fe/MgO/Fe magnetic tunnel junctions**, *Nat. Mater.* 3 (2004) 868–871.
<https://doi.org/10.1038/nmat1257>
- [41] S. S. P. Parkin, C. Kaiser, A. Panchula, P. M. Rice, B. Hughes, M. Samant, S.-H. Yang, **Giant tunnelling magnetoresistance at room temperature with MgO (100) tunnel barriers**, *Nat. Mater.* 3 (2004) 862–867.
<https://doi.org/10.1038/nmat1256>
- [42] W. F. Brown, **Thermal Fluctuations of a Single-Domain Particle**, *Phys. Rev.* 130 (1963) 1677–1686.
<https://doi.org/10.1103/PhysRev.130.1677>
- [43] H. B. Callen, T. A. Welton, **Irreversibility and Generalized Noise**, *Phys. Rev.* 83 (1951) 34–40.
<https://doi.org/10.1103/PhysRev.83.34>
- [44] H. B. Callen, R. F. Greene, **On a Theorem of Irreversible Thermodynamics**, *Phys. Rev.* 86 (1952) 702–710.
<https://doi.org/10.1103/PhysRev.86.702>
- [45] H. B. Callen, M. L. Barasch, J. L. Jackson, **Statistical Mechanics of Irreversibility**, *Phys. Rev.* 88 (1952) 1382–1386.
<https://doi.org/10.1103/PhysRev.88.1382>
- [46] R. F. Greene, H. B. Callen, **On a Theorem of Irreversible Thermodynamics. II**, *Phys. Rev.* 88 (1952) 1387–1391.
<https://doi.org/10.1103/PhysRev.88.1387>